Nanosecond radio bursts from strong plasma turbulence in the Crab pulsar

T. H. Hankins*, J. S. Kern*†, J. C. Weatherall* & J. A. Eilek*

** Physics Department, New Mexico Tech, and † National Radio Astronomy Observatory, Socorro, New Mexico 87801, USA*

The Crab pulsar was discovered[1] by the occasional exceptionally bright radio pulses it emits, subsequently dubbed 'giant' pulses. Only two other pulsars are known to emit giant pulses[2,3]. There is no satisfactory explanation for the occurrence of giant pulses, nor is there a complete theory of the pulsar emission mechanism in general. Competing models for the radio emission mechanism can be distinguished by the temporal structure of their coherent emission. Here we report the discovery of isolated, highly polarized, two-nanosecond subpulses within the giant radio pulses from the Crab pulsar. The plasma structures responsible for these emissions must be smaller than one metre in size, making them by far the smallest objects ever detected and resolved outside the Solar System, and the brightest transient radio sources in the sky. Only one of the current models—the collapse of plasma-turbulent wave packets in the pulsar magnetosphere—can account for the nanopulses we observe.

We have carried out wideband, ultrahigh time resolution observations of the Crab giant pulses at the Arecibo Observatory's 305-m telescope. We developed a new data acquisition system, which we used at 5.5 and 8.6 GHz with bandwidths of 0.5 and 1 GHz. Data acquisition is inhibited by our system during the 30–40 s required to transfer the 8 or 16 million samples per pulse from acquisition memory to computer disk storage for offline processing. Our sample of giant pulses is therefore incomplete. However, the pulses exceeded our detection threshold typically once per minute or less, so few strong pulses were missed.

To attain nanosecond time resolution, we must fully account for the interstellar propagation effects that distort pulsar signals: dispersion, Faraday rotation and interstellar scattering broadening. The frequency-dependent delay caused by dispersive propagation through the tenuous interstellar plasma is corrected using the coherent dispersion removal technique[4,5]. Faraday rotation is less than ten degrees across the receiver bandwidth, and scattering broadening is negligible above 5 GHz. Hence, propagation effects do not limit our time resolution.

The radio spectrum of the Crab giant pulses is steep[6], and the radio pulses do not appear to be associated with high-energy emissions at X-ray or gamma-ray frequencies[7]. At low radio frequencies where their energies are greatest, propagation effects obliterate the detailed pulse structure. Hence, to test the detailed theoretical predictions of the emission signature, we must observe at the highest practical frequencies, where the pulses are still pristine and the lack of terrestrial radio interference permits wide receiver bandwidths.

A set of six giant pulses, which were recorded over a span of a few minutes, is shown in Fig. 1. The arrival time of a giant pulse, or the pulse phase, relative to a fixed point on the rotating star's surface, jitters from one giant pulse to another by several hundred microseconds. However, the pulse phases are confined to the main pulse and interpulse regions of the mean profile, which is formed by averaging the intensity synchronously with the rotation period. The pulses shown here are all near the phase of the main pulse. Most of the pulses show one or more noisy bursts separated by fractions of microseconds. After coherent dedispersion, we find that the intrinsic duration of the giant pulses is extremely short; their total widths are typically less than 1 μs above 5 GHz (interstellar scattering broadening dominates the pulse widths below 1 GHz), and they contain clear structure down to the inverse bandwidth time limit. The intensity autocorrelation of the giant pulses shows a characteristic width (the width of the first inflection point, excluding the amplitude of the noise 'spike' at zero lag due to the uncorrelated receiver noise and unresolved structure) of approximately 200 ns at 5.5 and 8.6 GHz.

Pulsar radio emission has been modelled as amplitude-modulated noise[8,9] where a wideband noise process, $n(t)$, is modulated by a more slowly varying amplitude function, $a(t)$. The noise process is produced by the ensemble of N 'shot' pulses, which occur randomly in the (receiver) time resolution interval, Δt. The duration of the shot pulses is related to the inverse of the pulsar spectral bandwidth, which is assumed to extend beyond $1/\Delta t$. For large N, $n(t)$ approaches a gaussian random process by the Central Limit theorem. But if the receiver resolution Δt is small enough, $N \approx 1$, the individual shots are resolved, and the observed noise process has non-gaussian statistics.

For the typical observed pulse $N \gg 1$, and the pulse is consistent with the amplitude-modulated noise model. But occasionally we record a pulse lasting tens of microseconds that is composed of extremely short, isolated, non-overlapping impulses, such as pulse 3 in Fig. 1. For these pulses $N \leq 1$, and we can distinguish individual nanopulses. In Fig. 2 we have expanded portions of pulse 3 to show the wealth of detail down to the $\Delta t = 2$ ns resolution limit imposed by the 500-MHz receiver bandwidth. We plot the right and left circular polarizations separately. It is clear that these nanopulses are strongly circularly polarized, the polarization can be of either hand, and can change hands in a few microseconds. Some giant pulses from the millisecond pulsar B1937 + 214 are known to be circularly

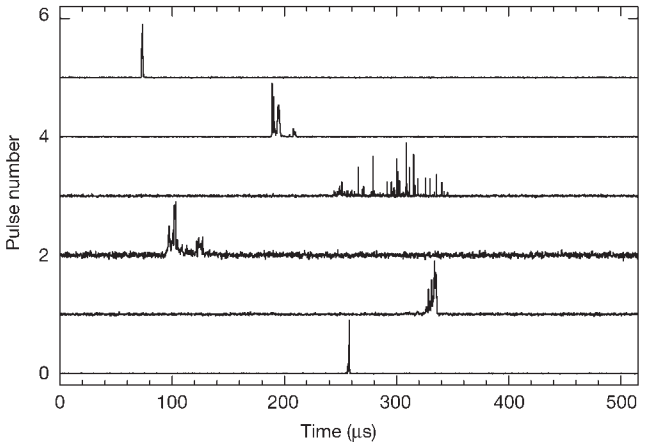

Figure 1 A sequence of dedispersed Crab giant pulses. The arrival time jitter and varied shapes of the total intensity are shown. The time axis origin is modulo one pulsar rotation period. Each pulse has been plotted with a time resolution of 250 ns and is normalized to the same maximum amplitude. The centre frequency is 5.5 GHz and the sampled bandwidth is 0.5 GHz. A square-law power detector with a 200-μs time constant was used to detect the presence of a giant pulse in the receiver pass band. A 2-ms time window, synchronous with the Doppler-shifted main pulse arrival times, was obtained from our separate pulsar timing system. When the detected intensity exceeded a preset threshold of eight times the r.m.s. off-pulse noise during the main pulse 2-ms window, a giant pulse was captured by digitally sampling the voltage of both orthogonal polarizations at 1 or 2×10^9 samples per second using a LeCroy 9354L or LC584L digital oscilloscope. Offline, the critically sampled signals are passed through a software filter whose transfer function inverts the interstellar dispersion. The resulting time resolution is the reciprocal of the receiver bandwidth, ultimately 1–2 ns. The dedispersion process redistributes the power of any impulsive terrestrial interference over the filter impulse response time, which for these data is 1.42 ms, or 1,420,000 samples, thus reducing its impact on the pulsar signal.

polarized and can have both signs of circular polarization[2]. Some of the nanopulses we observe are possibly shorter than 2 ns. Their intensities often exceed 10^3 Jy for extremely brief intervals, placing them only after the Sun as the brightest objects in the centimetre wavelength radio sky.

Assuming a distance to the Crab pulsar of 2.0 kpc, and an emitting source diameter $d = c\Delta t = 60$ cm, the equivalent brightness temperature of the source is 10^{37} K. This very high value for the brightness temperature implies that the emission is coherent. The energy density in a 1,000-Jy pulse of 2-ns duration is about 2×10^{14} erg cm^{-3}. For comparison, standard pulsar electrodynamics[10] allows us to estimate the energy density of the emitting plasma. From the charge density necessary to maintain the electric field that allows the plasma to co-rotate with the star, we obtain the number density if the plasma contains only one charge sign. If we assume the Lorentz factor of charges that initially leave the Crab pulsar is $\gamma \approx 10^7$, we obtain a plasma energy density of around 6×10^{13} erg cm^{-3}. That the plasma energy density is not significantly larger than the radiation energy density clearly implies a nonlinear, collective emission process.

Statistical analysis of phase- and frequency-dependent attributes of the signals indicates that giant pulses are true temporal modulations rather than an angular beaming effect[7,11]. If the giant pulse duration were due to the angular sweep of a beam past the observer[12], then the relativistic factor of the emitter would have to be $\gamma \approx 10^6$. Although this is comparable to the energies reached by particles initially leaving the star, in most models the radio emission is produced from a slower, denser pair plasma. Models of the pair cascade, which conserve the energy density of the initial plasma, predict much slower particle flows[13], typically $\gamma \leq 10^3$, and therefore angular beaming is an unlikely explanation for the short time structure we observe.

If the very short nanopulses we observe are the fundamental elements of the emission, then they must result directly from the microphysics of the radio emission process. The broad categories of processes capable of producing high brightness radio emission in pulsars—spatially coherent curvature emission[14], plasma turbulence[15,16], and masers[17,18]—can be tested on the basis of their behaviour on these timescales. The short timescale observations open a new window on the pulsar emission process not accessible to previous statistical studies[19–21] that attempted to test the emission mechanism.

In direct emission mechanisms such as curvature radiation, spatial structure occurs as electrons are trapped in bunches in the potential troughs of a large-amplitude plasma wave. The emitting entity is a periodic train of bunches, of coherence length $s_0 \approx c/\Delta\nu$. For a linear column with a sinusoidal charge perturbation, the intensity of the emission is proportional to $(\langle\sigma\rangle s_0)^2$, where $\langle\sigma\rangle$ is the root-mean-square (r.m.s.) charge density of the perturbation[13]. Thus, coherent trains of short s_0 will emit less effectively than longer ones. Also, as s_0 increases, the intensity spikes grow more intense, but also narrower in frequency. On the basis of this model, Benford[22] predicted that radio structure of bandwidth greater than 100 kHz would not exist, and hence one would expect no temporal features shorter than about 10 μs. Clearly, this is in contrast to our observations. Alternatively, a reduction in coherence length of a longer ensemble of bunches could produce shorter timescale fluctuations, but a mechanism to do this has not been established.

A similar problem is inherent in maser emission models. Non-gaussian coherence effects in masers[23,24] are possible on timescales down to the inverse of the maser bandwidth, $\Delta\nu^{-1}$. On the basis of our observed short timescale structure, $\Delta t \approx 2$ ns, a maser-like mechanism must have very wide band emission, $\Delta\nu \approx 1$ GHz. Relativistic plasma masers can interact with a broad spectrum of incoherent waves[16,17]. However, the high brightness temperature of the transient pulses requires a long coherence path length. But, because the growth rate varies across the spectrum, the band-

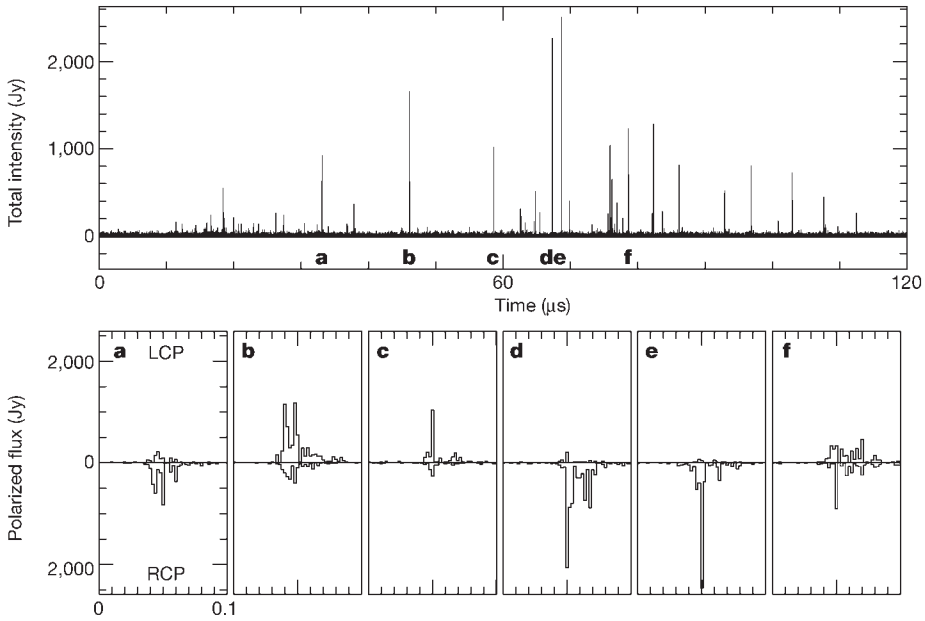

Figure 2 Intensity, polarization and time structure of nanopulses. The upper panel shows details of pulse 3 in Fig. 1, plotted with 2-ns resolution. Sections of 100-ns duration showing the polarized flux from six of the nanopulses, labelled **a**–**f**, are plotted below with left circular polarization upward, and right circular polarization downward, also with 2-ns resolution. The r.m.s. noise level is 18 Jy. The temporal interstellar scattering broadening, τ_{ISS}, due to multipath propagation through the turbulent Crab nebula and the interstellar medium, is negligible; scaling our own previously measured 0.33 and 1.4 GHz values as $\nu^{-4.4}$ (Kolmogorov spectrum), we expect $\tau_{ISS} = 1.9$ ns at 5.5 GHz, and 0.2 ns at 8.6 GHz. These values are roughly consistent with interstellar scattering model predictions (J. M. Cordes and T. J. W. Lazio, personal communication) of $\tau_{ISS} = 0.5$ and 0.05 ns for $\nu = 5.5$ and 8.6 GHz, respectively.

width decreases with increasing path length. A numerical model[17] for one relativistic plasma maser indicates a bandwidth that decreases to 20% for a brightness temperature of 10^{20} K. Thus, for masers, high brightness tends to be incompatible with broad bandwidth.

Emission in strong plasma turbulence is associated with the nonlinear localization of electrostatic wave energy in the plasma source region, and the subsequent explosive collapse of wave packets that takes place over a few wave oscillation periods[25,26]. Numerical modelling[27] of individual pulses produced by strong plasma turbulence at 5 GHz predicts nanosecond radio bursts, and quasi-periodic structure due to resonant coupling between the plasma and radiative modes on the timescale of 1–3 ns, in agreement with our observations. Plasma turbulence is the only pulsar emission model for which a mechanism has been identified that can produce such extremely short giant radio pulses. We conclude, therefore, that giant pulse radio emission from the Crab pulsar results from the conversion of electrostatic turbulence in the pulsar magnetosphere by the mechanism of spatial collapse of nonlinear wavepackets.

The nanopulses we have detected represent an example of highly efficient coherent radio emission from a relativistic flow that serves as a prototype for coherent, transient radio emission from perhaps a larger class of sources, such as active galactic nuclei. Although extraordinary attention has been given to transients in X-ray[28] and gamma-ray wavelengths, radio transients represent a largely unexplored observational regime[29]. Indeed, the techniques we apply to recover the Crab giant pulses will be useful in the search for extrasolar radio bursts and pulsars in other galaxies. □

Received 8 July 2002; accepted 4 February 2003; doi:10.1038/nature01477.

1. Staelin, D. H. & Reifenstein, E. C. III Pulsating radio sources near the Crab nebula. *Science* **162,** 1481–1483 (1968).
2. Cognard, I., Shrauner, J. A., Taylor, J. H. & Thorsett, S. E. Giant radio pulses from a millisecond pulsar. *Astrophys J.* **457,** L81–L84 (1996).
3. Romani, R. W. & Johnston, S. Giant pulses from the millisecond pulsar B1821–24. *Astrophys J.* **557,** L93–L96 (2001).
4. Hankins, T. H. Microsecond intensity variations in the radio emissions from CP 0950. *Astrophys J.* **169,** 487–491 (1971).
5. Hankins, T. H. & Rickett, B. J. Pulsar signal processing. *Meth. Comp. Phys.* **14,** 55–129 (Academic, New York, 1975).
6. Sallmen, S., Backer, D. C., Hankins, T. H., Moffett, D. & Lundgren, S. Simultaneous dual-frequency observations of giant pulses from the Crab pulsar. *Astrophys. J.* **517,** 460–471 (1999).
7. Lundgren, S. C. *et al.* Giant pulses from the Crab pulsar: A joint radio and gamma-ray study. *Astrophys. J.* **453,** 433–446 (1995).
8. Rickett, B. J. Amplitude-modulated noise: An empirical model for the radio radiation received from pulsars. *Astrophys. J.* **197,** 185–191 (1975).
9. Cordes, J. M. Pulsar radiation as polarized shot noise. *Astrophys. J.* **210,** 780–791 (1976).
10. Goldreich, P. & Julian, W. H. Pulsar electrodynamics. *Astrophys. J.* **157,** 869–880 (1969).
11. Rickett, B. J. & Cordes, J. M. in *Pulsars, IAU Symp. 95* (eds Sieber, W. & Wielebinski, R.) 107–109 (Reidel, Boston, 1981).
12. Popov, M. V. *et al.* Microstructure of pulsar radio pulses measured with a time resolution of 62.5 ns at 1650 MHz. *Astron. Rep.* **46,** 206–213 (2002).
13. Arendt, P. N. Jr & Eilek, J. A. Pair creation in the pulsar magnetosphere. *Astrophys. J.* **581** (in the press).
14. Buschauer, R. & Benford, G. General theory of coherent curvature radiation. *Mon. Not. R. Astron. Soc.* **177,** 109–136 (1976).
15. Asseo, E., Pelletier, G. & Sol, H. A non-linear radio pulsar emission mechanism. *Mon. Not. R. Astron. Soc.* **247,** 529–548 (1990).
16. Weatherall, J. C. Modulational instability, mode conversion, and radio emission in the magnetized pair plasma of pulsars. *Astrophys. J.* **483,** 402–413 (1997).
17. Lyutikov, M., Blandford, R. D. & Machabeli, G. On the nature of pulsar radio emission. *Mon. Not. R. Astron. Soc.* **305,** 338–352 (1999).
18. Weatherall, J. C. A relativistic-plasma Compton maser. *Astrophys. J.* **559,** 196–200 (2001).
19. Jenet, F. A., Anderson, S. B. & Prince, T. A. The first detection of coherent emission from radio pulsars. *Astrophys. J.* **558,** 302–308 (2001).
20. Cairns, I. H., Johnston, S. & Das, P. Intrinsic variability of the Vela pulsar: Lognormal statistics and theoretical implications. *Astrophys. J.* **563,** L65–L68 (2001).
21. Delaney, T. & Weatherall, J. C. Model for deterministic chaos in pulsar radio signals and search for attractors in the Crab and Vela pulsars. *Astrophys. J.* **519,** 291–302 (1999).
22. Benford, G. Model for the microstructure emission of pulsars. *Mon. Not. R. Astron. Soc.* **179,** 311–315 (1977).
23. Elitzur, M. *Astronomical Masers* 68–71 (Kluwer, Boston, 1992).
24. Moran, J. M. Statistical properties of the radiation fields from H_2O masers. *Bull. Am. Astron. Soc.* **13,** 508 (1981).
25. Zakharov, V. E. Collapse of Langmuir waves. *Sov. Phys. JETP* **35,** 908–914 (1972).
26. Goldman, M. V. Strong turbulence of plasma waves. *Rev. Mod. Phys.* **56,** 709–735 (1984).
27. Weatherall, J. C. Pulsar radio emission by conversion of plasma wave turbulence: Nanosecond time structure. *Astrophys. J.* **506,** 341–346 (1998).
28. Strohmayer, T. E., Swank, J. H. & Zhang, W. in *The Active X-ray Sky: Results from BeppoSAX and RXTE* (eds Scarsi, L., Bradt, H., Giommi, P. & Fiore, F.) *Nucl. Phys. B (Proc. Suppl.)* **69**, 129 (1997).
29. Mészáros, P. Gamma-ray bursts: Accumulating afterglow implications, progenitor clues, and prospects. *Science* **291,** 79–84 (2001).

Acknowledgements T.H.H. thanks NRAO and NAIC for partial sabbatical leave support at the Green Bank and Arecibo Observatories. J.S.K. thanks NRAO for pre-doctoral support. We thank B. Driggers of TMS and LeCroy for the loan of a LeCroy LT584L oscilloscope, J. Ford at NRAO Green Bank for square-law detectors, NRAO Socorro for computer support and technical assistance, and the NSF for a research grant. The Arecibo Observatory is operated by Cornell University under a cooperative agreement with the National Science Foundation.

Competing interests statement The authors declare that they have no competing financial interests.

Correspondence and requests for materials should be addressed to T.H.H. (e-mail: thankins@aoc.nrao.edu).

An extended upper atmosphere around the extrasolar planet HD209458b

A. Vidal-Madjar*, A. Lecavelier des Etangs*, J.-M. Désert*, G. E. Ballester†, R. Ferlet*, G. Hébrard* & M. Mayor‡

** Institut d'Astrophysique de Paris, CNRS/UPMC, 98bis boulevard Arago, F-75014 Paris, France*
† Lunar and Planetary Laboratory, University of Arizona, 1040 E. 4th St., Rm 901, Tucson, Arizona 85721-0077, USA
‡ Observatoire de Genève, CH-1290 Sauverny, Switzerland

The planet in the system HD209458 is the first one for which repeated transits across the stellar disk have been observed[1,2]. Together with radial velocity measurements[3], this has led to a determination of the planet's radius and mass, confirming it to be a gas giant. But despite numerous searches for an atmospheric signature[4–6], only the dense lower atmosphere of HD209458b has been observed, through the detection of neutral sodium absorption[7]. Here we report the detection of atomic hydrogen absorption in the stellar Lyman α line during three transits of HD209458b. An absorption of 15 ± 4% (1σ) is observed. Comparison with models shows that this absorption should take place beyond the Roche limit and therefore can be understood in terms of escaping hydrogen atoms.

Far more abundant than any other species, hydrogen is well-suited for searching weak atmospheric absorptions during the transit of an extrasolar giant planet in front of its parent star, in particular over the strong resonant stellar ultraviolet Lyman α emission line at 1,215.67 Å. Depending upon the characteristics of the planet's upper atmosphere, an H I signature much larger than that for Na I at 0.02% (ref. 7) is foreseeable. Three transits of HD209458b (named A, B and C hereafter) were sampled in 2001 (on 7–8 September, 14–15 September and 20 October, respectively) with the Space Telescope Imaging Spectrograph (STIS) onboard the Hubble Space Telescope (HST); the data set is now public in the HST archive. To partially overcome contamination from the Earth's Lyman α geocoronal emission, we used the G140M grating with the $52'' \times 0.1''$ slit (medium spectral resolution: $\sim$20 km s^{-1}). For each transit, three consecutive HST orbits (named 1, 2 and 3 hereafter) were scheduled such that the first orbit (1,780 s exposure) ended before the first contact to serve as a reference, and the two following